Materials Science & Engineering A 729 (2018) 208–218

Contents lists available at ScienceDirect

Materials Science & Engineering A

journal homepage: www.elsevier.com/locate/msea

Solid solution softening and enhanced ductility in concentrated FCC silver solid solution alloys

Yongjun Huo[a,b,*], Jiaqi Wu[a,b], Chin C. Lee[a,b]

[a] Electrical Engineering and Computer Science University of California, Irvine, CA 92697-2660, United States
[b] Materials and Manufacturing Technology University of California, Irvine, CA 92697-2660, United States

ARTICLE INFO

Keywords:
Concentrated solid solutions
Solid solution softening
Twinning-induced plasticity
Localized homologous temperature
Advanced joining materials

ABSTRACT

The major adoptions of silver-based bonding wires and silver-sintering methods in the electronic packaging industry have incited the fundamental material properties research on the silver-based alloys. Recently, an abnormal phenomenon, namely, solid solution softening, was observed in stress vs. strain characterization of Ag-In solid solution. In this paper, the mechanical properties of additional concentrated silver solid solution phases with other solute elements, Al, Ga and Sn, have been experimentally determined, with their work hardening behaviors and the corresponding fractography further analyzed. Particularly, the concentrated Ag-Ga solid solution has been discovered to possess the best combination of mechanical properties, namely, lowest yield strength, highest ductility and highest strength, among the concentrated solid solutions of the current study. Microscopically, a clear evidence of narrow twin lamella feature has been observed in the Ag-Ga solid solution, and further identified as the deformation twinning, using high resolution transmission electron microscopy (HRTEM). To explain solid solution softening mechanism in low Peierls potential FCC metals, the authors have proposed a self-contained theoretical interpretation associated with fractional kink-pairs formation, and originally introduced the concept of the short range order (SRO) induced localized homologous temperature (LHT). Furthermore, the mechanism of twinning-induced plasticity (TWIP) can be referred as the underlying reason of the enhanced ductility in the Ag-Ga solid solution alloy. With such excellent mechanical properties, the Ag-Ga solid solution alloy is expected to have a great potential in the development of advanced joining materials for the various applications in electronics industries.

1. Introduction

In early days of metallurgical science, silver solid solutions with various solute elements were the subjects of research study to learn their material properties, such as the lattice constants [1] and elastic constants [2]. Solid solution hardening is a well-known mechanism to explain the increase of yield strength and hardness of alloys due to the interactions between dislocations and solute atoms. Within Fleischer's continuum elasticity scheme [3], the lattice distortion induced by the solute atoms create local hydrostatic stress field which can behave as an obstacle for the gliding movement of dislocations, thereby postponing the onset of material yielding point. Generally speaking, the types of interactions can be qualitatively classified into the following categories: elastic interaction, modulus interaction, stacking-fault interaction, electrical interaction, short-range order (SRO) and long-range order (LRO) interactions [4]. It has been tried to establish a theoretical model [5] in order to get a better picture of the nature of silver and other face centered cubic (FCC) solid solutions mechanical behaviors with their guiding mechanisms, however, the results were rather inconclusive. The complexity lies in the random nature of the disordered solid solution alloys. Possibly due to the fact that silver and its solid solution alloys were not seriously considered as structural materials, the understandings on their mechanical properties, especially plasticity, were relatively limited. With the fast development of integrated circuit (IC) industries, electronic manufacturing and packaging activities have already grown into a global market of hundreds of billions of dollars per year. Recently, silver-based solid solution alloys have been widely considered as an alternative of interconnection materials in electronics manufacturing and packaging applications, such as die-attachment [6,7] and wire-bonding [8,9]. The mechanical properties are crucial to the manufacturability of the materials and long-term reliability of the whole electronic system. Therefore, the fundamental study on the mechanical properties of silver solid solution alloys has become very meaningful to the real industrial applications.

In our recent research, the authors have studied the mechanical properties of concentrated silver-indium (Ag-In) solid solution alloy

* Corresponding author at: Electrical Engineering and Computer Science University of California, Irvine, CA 92697-2660, United States.
E-mail addresses: yongjunh@uci.edu (Y. Huo), jiaqw10@uci.edu (J. Wu), cclee@uci.edu (C.C. Lee).

https://doi.org/10.1016/j.msea.2018.05.057
Received 8 January 2018; Received in revised form 17 April 2018; Accepted 17 May 2018
Available online 18 May 2018
0921-5093/

[10], which is considered to be one of the promising candidates for metallic interconnection applications in electronic packaging, owing to its excellent mechanical properties and its great anti-tarnishing property [11]. During the investigation on Ag-In binary system, the authors found an interesting phenomenon, called solid solution softening, showing an unusual and opposite mechanical behaviors to the traditional solid solution hardening theorem. Solid solution softening phenomenon was firstly discovered, and extensively studied in body centered cubic (BCC) metal alloys [12]. It was also found in intermetallics [13], semiconductors [14], and ceramic [15], whereas its experimental report on FCC metals was relatively seldom. The lower yield strength is a very desirable material property in the applications associated with solid-state bonding. It allows the heterogeneous-bonded structure to curtail the thermal stresses, induced by coefficient of thermal expansion (CTE) mismatch [16], with an easier plastic deformation process, thereby preventing electronic devices from cracking and mechanical failures [17]. Therefore, solid solution softening is an attractive behavior in the utilization of heterogeneous structure integration when manufacturing the electronics. In addition, a considerable enhancement of ductility has been found in the Ag-In concentrated solid solution alloy, as compared with pure Ag. The enhanced ductility is also a favorable material property for the improvement of the manufacturability and mechanical shock stability. Yet, the underlying mechanisms of solid solution softening and enhanced ductility must be understood before safely applied to the industrial volume production. In the present work, the authors continue to investigate on the mechanical behaviors of additional Ag-based solid solution alloys, in order to rationalize the phenomenological nature of the solid solution softening and the enhanced ductility with theoretical considerations, in the meanwhile, exploring for more potential jointing material candidates for the electronic packaging utility.

In the following sessions, the authors first briefly describe the material preparation and experimental methods, such as X-ray diffraction (XRD), scanning electron microscope/energy dispersive X-ray spectroscopy (SEM/EDX), transmission electron microscopy (TEM) and stress vs. strain characterization in the tensile test, followed by their experimental results with detailed analysis. Furthermore, the solid solution softening and enhanced ductility behaviors in the concentrated FCC silver solid solution alloys has been extensively discussed in a systematically and theoretically manner. An original insight has been provided in order to establish the theoretical correlations between the macroscopic material behaviors and the corresponding microscopic material structures. Finally, the advantages of the concentrated FCC silver solid solution alloys have been suggested in the applications of the electronic manufacturing and packaging industries.

2. Material and methods

2.1. Materials synthesis

Initially, the authors observed that the (Ag)-9.5In (9.5 at%) exhibited the solid solution softening behavior in Ag-In binary system. A question was raised naturally: does this solid solution softening mechanism exist only in Ag-In binary system or in other Ag-based solid solutions as well? Since our research starting point is Ag solid solution phase with In solute, the authors decided to choose common metallic elements in the IIIA column of periodic table, same as In, namely, Al and Ga, as potential candidates of solute elements. In addition, Sn was chosen as it is the next element after In. Cadmium (Cd), the element before In, was seriously considered but not chosen because it is one of the banned elements by Restriction of Hazardous Substances (RoHS) in electronic products utility.

It is constructive to review Ag-Al, Ag-Ga, and Ag-Sn phase diagrams before preparing each single phase Ag solid solutions in these three binary systems. According to Ag-Al [18], Ag-Ga [19], and Ag-Sn [20] binary phase diagrams, the maximum solubility of Al, Ga and Sn elements in silver crystal at room temperature are about 10 at% (2.6 wt %), 10 at% (6.6 wt%), and 8 at% (8.7 wt%), respectively. Solid solution softening usually occurs in solid solutions with high concentration of solute element, which is exactly the case in Ag-In binary system. Therefore, the authors decided to grow Ag-Al and Ag-Ga concentrated solid solution ingots with solute concentration near 10 at%, and Ag-Sn concentrated solid solution ingots with solute concentration near 8 at%, using the vacuum casting method. The grown materials are nominally designated as (Ag)-10Al, (Ag)-10Ga, and (Ag)-8Sn in this paper, respectively. Raw materials with 99.99 wt% purity of Ag shots together with Al, Ga, Sn shots, respectively, were weighed, uniformly mixed and loaded in quartz tubes with one end closed. While the quartz tube was being pumped by a vacuum pump, the other end of the tube was sealed by hydrogen-oxygen torch operation to form a capsule. The vacuum environment is essential for the casting production to mitigate material oxidation issues, the number of voids, and common defects created by trapped air bubbles. Next, the capsules were placed into a furnace preheated at 1030 °C and stayed there for 30 min. The temperature of the furnace was then reduced gradually to room temperature in 7 days in order to obtain the homogenized single phase Ag-Al, Ag-Ga, and Ag-Sn solid solutions at desired compositions. After successful production of (Ag)-10Al, (Ag)-10Ga, and (Ag)-8Sn ingots, they were cut into disk samples using slow speed diamond saw and polished with a sequence of 120/240/600/800/1200 grits of silicon carbide abrasive papers for further chemical composition examinations and crystal structure evaluations.

2.2. X-ray diffraction characterization

XRD was used to identify the phases and to measure the lattice constants of the grown bulk materials. Rigaku SmartLab X-ray diffractometer in Irvine Material Research Institute (IMRI) was used for phase identification, using Bragg-Brentano (BB) operation mode with θ-θ diffractometer setting. Bragg-Brentano optics setting was chosen since the disk samples from ingots were bulk polycrystalline materials. The XRD is performed from 30° to 90° at scanning speed of 2°/min with scanning step width of 0.02°, using collimated Cu K_α line excitation X-ray source, with a filter removing Cu K_β line. After XRD measurement, the collected data were analyzed by PDXL, an integrated powder X-ray analysis software package, and compared with The International Center for Diffraction Data (ICDD) standard card.

2.3. Scanning electron microscopy and energy dispersive X-ray spectroscopy

The SEM imaging pictures in this paper were taken at 10 kV electron beam voltage with secondary electron (SE) mode using Everhart-Thornley (ET) detector in order to capture the morphology of the samples. Chemical compositions were examined quantitatively with SEM/EDX with FEI XL-30 SEM in IMRI, arbitrarily chosen from multiple areas on the disk samples. In order to determine the averaged solute concentration at each areas, the EDX spectrum mapping mode was used with ZAF correction method at 20 kV electron beam voltage and 33.7° take-off angle. The quantification results of SEM/EDX spectrum mapping were then collected and summarized with the information of average solute concentration and machine error.

2.4. Transmission electron microscopy

In order to study the correlations between the macroscopic mechanical properties and the microscopic material structures, transmission electron microscopy (TEM) was used to provide direct experimental evidences for the further theoretical interpretations. JEOL JEM-2100F TEM with Schottky type field emission gun, operating at 200 kV, was used in this study. Gatan K2 direct detection camera was used to capture TEM micrographs and selected area electron diffraction (SAED) patterns. TEM samples were prepared from the grown bulk materials,

using the traditional grinding-dimpling method. Manual grinding was performed on the TEM samples in order to create a certain degree of plastic deformation. Finally, Gatan PIPs ion miller was used for the final thinning of the TEM samples to the electron transparency thickness with minimum material damage.

2.5. Tensile test experimental setting

Tensile test samples, conforming with American Society for Testing and Materials (ASTM) standard E8/ E8M- 08 [21], were prepared using electrical discharge machining (EDM) by an outsource company. The geometry and dimensions of the samples were the same, as described elsewhere in the previous works [10]. EDM process can change the surface properties of the workpiece, causing the issues such as re-casting, heat affected zone (HAZ) grain size enlargement. Therefore, tensile test samples were polished slightly to remove the HAZ layer. Then, the tensile test samples were put into an oven and annealed at 200 °C for an hour to release the residue internal stresses induced by the polishing process. After the preparation, tensile test samples were examined, using XRD approach mentioned previously with the same setting. By comparing the XRD patterns with previous results, the authors can confirm that the tensile test samples have the same compositions as the disk samples examined by the XRD and SEM/EDX analysis.

The tensile test was performed using Instron model 5500 R tensile tester with the deformation speed of 10^{-4} mm/s at controlled software panel setting. Since the size of manufactured tensile test samples may vary a little bit from the original design, all of the critical dimensions, such as the length, width, and thickness of the tested region, were calibrated at the control software panel. The true strain rate was around 10^{-5}/s, within the range of static tension test condition. The raw data of engineering stress and strain were recorded automatically by the controlled software for the following data analysis.

3. Experimental results

3.1. X-ray diffraction characterization results

As shown in Fig. 1, the XRD patterns of (Ag)-10Al, (Ag)-10Ga and (Ag)-8Sn disk samples were plotted together with the ones of pure Ag and (Ag)-9.5In. It is very clear that (Ag)-10Al, (Ag)-10Ga and (Ag)-8Sn resemble the crystal structure of pure Ag, i.e., FCC structure, from their typical systematically peaks absence. There are no peaks other than the peaks of (Ag)-10Al, (Ag)-10Ga and (Ag)-8Sn in each XRD patterns. Therefore, it can be safely concluded that the disk samples are single phase and polycrystalline materials. The calculated average values for lattice constants are 4.084 Å, 4.088 Å and 4.129 Å for (Ag)-10Al, (Ag)-10Ga and (Ag)-8Sn, respectively. The lattice constants of pure Ag and (Ag)-9.5In have the values of 4.094 Å and 4.126 Å, as measured in the previous work [10]. As shown in Fig. 2, the calculated average values of concentrated Ag solid solution alloys were plotted together for each solute elements. In the Fig. 1, the XRD patterns of (Ag)-10Al and (Ag)-10Ga shifted towards right, whereas the XRD patterns of (Ag)-9.5In and (Ag)-8Sn shifted towards left, compared to that of pure Ag. The substitution of Ag atoms with Al and Ga solutes resulted in dent in its original crystal lattice, creating a compressive strain core at each substitutional sites. Therefore, the values of average lattice constants of (Ag)-10Al and (Ag)-10Ga decreased from that of pure Ag. In contrast, the substitution of Ag atoms with In or Sn solutes bulged its original crystal lattice, increased the average lattice constants, and created a tensile strain core at each substitutional sites.

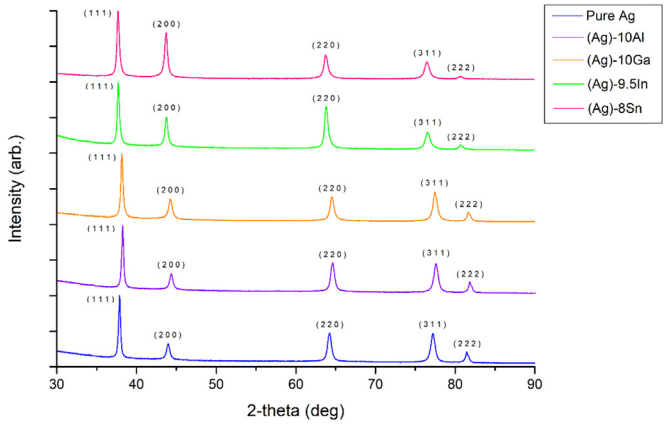

Fig. 1. XRD patterns of pure Ag and the concentrated Ag solid solution alloys with Al, Ga, In and Sn solute elements.

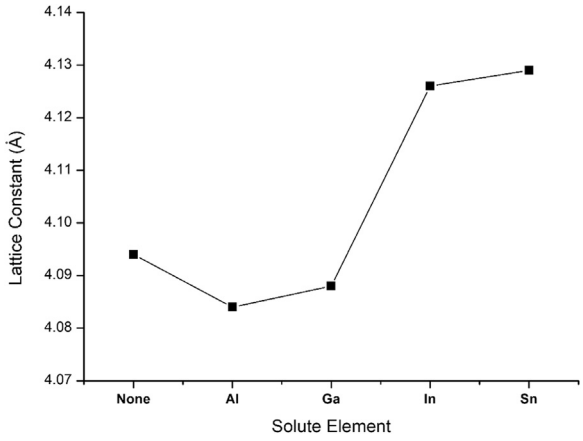

Fig. 2. The plot of calculated average lattice constants of pure Ag and the concentrated Ag solid solution alloys with Al, Ga, In and Sn solute elements.

3.2. Energy dispersive X-ray spectroscopy results

The quantification results of SEM/EDX spectrum mapping were summarized in Table 1 with the information of average concentration and machine error. As shown in Table 1, the average chemical compositions of (Ag)-10Al, (Ag)-10Ga and (Ag)-8Sn were very close to the nominal compositions with small systematic machine errors which were caused by the uncertainty of the SEM/EDX detector. Therefore, the authors confirmed that the grown ingots of (Ag)-10Al, (Ag)-10Ga and (Ag)-8Sn were nearly homogeneous at the designed solute concentrations, thereby proving that the initial nominal designations were indeed valid.

The bulk material samples were coarse-grained with similar grain size, after annealing for a long time with similar profiles. Now that the solute concentrations for different solid solutions are similar to each other, therefore, it is reasonable to assume the mechanical properties of the Ag-based concentrated solid solution alloys in this research as a single variable function of the solute elemental type.

3.3. Tensile test results

After collecting the raw data of engineering stress and strain from the tensile tests, the true stress and strain can be calculated using the Eq. (1) and Eq. (2) [22]:

$$\sigma_T = s(e+1) \tag{1}$$

$$\varepsilon_T = ln(e+1), \tag{2}$$

where s the engineering stress, e is the engineering strain, σ_T is the true stress, and ε_T is the true strain.

Representative raw data of tensile test results were plotted as the engineering stress-strain curves in Fig. 3, together with curves of pure

Table 1
SEM/EDX spectrum mapping quantification results of the chemical compositions for (Ag)-10Al, (Ag)-10Ga and (Ag)-8Sn disk samples.

	(Ag)-10Al		(Ag)-10Ga		(Ag)-8Sn	
	Ag (at%)	Al (at%)	Ag (at%)	Ga (at%)	Ag (at%)	Sn (at%)
Average concentration	90.3	9.7	90.1	9.9	91.7	8.3
Machine error	0.40	0.10	0.30	0.10	0.30	0.10

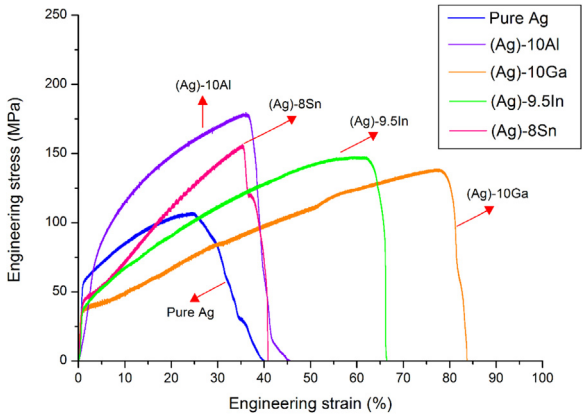

Fig. 3. The representative engineering stress-strain curves of (Ag)-10Al, (Ag)-10Ga, (Ag)-9.5In and (Ag)-8Sn with that of pure Ag in comparison.

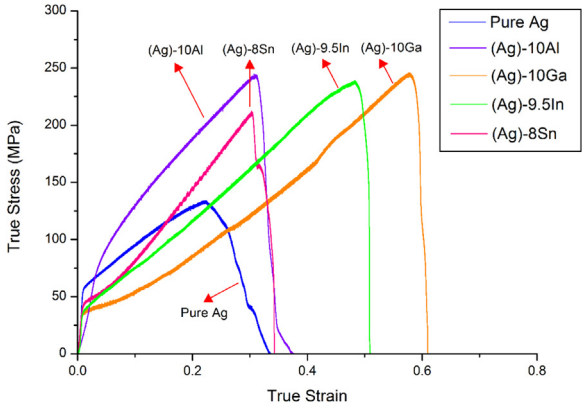

Fig. 4. The representative true stress-strain curves of (Ag)-10Al, (Ag)-10Ga, (Ag)-9.5In, and (Ag)-8Sn with that of pure Ag in comparison.

Table 2
A summary of mechanical properties of (Ag)-10Al, (Ag)-10Ga, (Ag)-9.5In and (Ag)-8Sn with pure Ag in comparison.

	Yield Strength (MPa)	Ultimate Tensile Strength (MPa)	True Uniform Strain (%)	True Fracture Strain (%)	Strain Hardening Index
Pure Ag	56.6	133.9	22.0	32.7	0.81
(Ag)-10Al	75.1	245.0	30.8	37.4	0.78
(Ag)-10Ga	34.5	246.1	57.5	60.8	1.32
(Ag)-9.5In	37.2	240.1	48.3	50.9	0.99
(Ag)-8Sn	42.3	212.6	30.2	34.2	1.27

Ag and (Ag)-9.5In obtained previously. By using Eqs. (1) and (2), the true stress and strain can be calculated for each data point, and the true stress vs. strain curves were plotted accordingly, as shown in Fig. 4. Mechanical properties of (Ag)-10Al, (Ag)-10Ga and (Ag)-8Sn can be further determined from the true stress vs. strain curves, namely, yield strength, ultimate tensile strength (UTS), true uniform strain (ε_u) and true fracture strain (ε_f) in tension stress status, summarized together with the data of pure Ag and (Ag)-9.5In in Table 2. Ultimate tensile strength describes how strong the material can possibly be after work hardening. The true uniform strain is the true strain at the maximum load, i.e., strain upon UTS point, which is often useful in estimating the ductility and formability of metals. In the plastic deformation region, the true stress can be also expressed mathematically in terms of yield stress and true plastic strain, depicted by Ludwik's equation [23], as shown in Eq. (3). With the data provided in Fig. 4, the strain hardening index, n, can be calculated, using Eq. (4), by examining the slope of $\log\sigma_p - \log\varepsilon_p$ curve. Then, the local strain hardening rate, R, for each stress vs. strain curve can be further determined by using Eq. (5).

$$\sigma_T = \sigma_y + K\varepsilon_p^n \tag{3}$$

$$n = \frac{d\log\sigma_p}{d\log\varepsilon_p} = \frac{\varepsilon_p}{\sigma_p}\frac{d\sigma_p}{d\varepsilon_p} \tag{4}$$

$$R = \frac{d\sigma_p}{d\varepsilon_p} = n\frac{\sigma_p}{\varepsilon_p}, \tag{5}$$

where σ_T is the true stress, σ_y is the yield stress, $\sigma_p = \sigma_T - \sigma_e$ is the true plastic stress, ε_T is the true strain, ε_e is the true elastic strain $\varepsilon_p = \varepsilon_T - \varepsilon_e$ is the true plastic strain, K is strength coefficient, and n is the strain hardening index. As a result, the calculated strain hardening indexes for (Ag)-10Al, (Ag)-10Ga and (Ag)-8Sn were also collected in Table 2. The stabilized strain hardening rates were plotted at each true plastic strain value, as shown in Fig. 5.

As shown in Fig. 4, although (Ag)-10Al, (Ag)-10Ga, (Ag)-9.5In, and (Ag)-8Sn are concentrated FCC solid solution alloys with similar solute concentrations, their corresponding stress vs. strain curves are quite different from each other. First of all, let us examine alloying effects on the yield strengths of those concentrated Ag solid solution alloys from stress vs. strain curves. The yield strengths can be determined from the true stress vs. strain curves, using 0.2% strain offset yield strength specification. The yield strength of (Ag)-10Al increases from 56.6 MPa to 75.1 MPa, whereas the yield strengths of (Ag)-10Ga and (Ag)-8Sn decrease to 34.5 MPa and 42.3 MPa, respectively. Therefore, it has proven that solid solution softening can also occur in Ag-Ga and Ag-Sn concentrated solid solution alloys, but not in Ag-Al system. Especially,

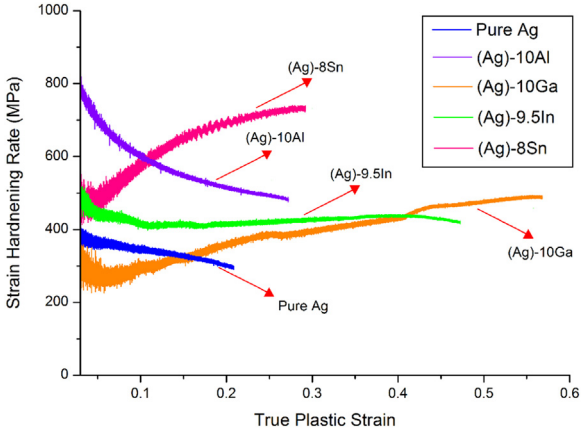

Fig. 5. The graphs of strain hardening rates of pure Ag, (Ag)-10Al, (Ag)-10Ga, (Ag)-9.5In, and (Ag)-8Sn.

the yield strength of (Ag)-10Ga is even lower than that of (Ag)-9.5In observed previously, so it is the lowest among the concentrated Ag solid solution alloys of current study.

Secondly, the work hardening behaviors of those concentrated Ag-based solid solution alloys are also different from each other, as depicted in Fig. 5. The initial work hardening of pure Ag is 380 MPa, and it decreases gradually as the plastic strain increases, to the value of 291 MPa at the end of the uniform plastic strain region. As shown in Fig. 4, the stress vs. strain curve of (Ag)-10Al has a very smooth transition from elastic region to plastic deformation stage. The initial strain hardening rate of (Ag)-10Al is 775 MPa, which is the highest among the five metals, and then it decreases to 479 MPa at the end of the uniform plastic strain region, with a shape of inverse parabola function. In contrast, (Ag)-10Ga has the sharpest elastic-to-plastic transition, followed by the onset of plastic deformation region with the lowest initial strain hardening rate, at the value of 292 MPa. Then, it increases almost linearly to the final value of 487 MPa. The initial strain hardening rate of (Ag)-9.5In has the value of 481 MPa. It decreases slightly, and then remains as a constant value around 420 MPa. The initial strain hardening rate of (Ag)-8Sn is 452 MPa. It increases with a shape of parabola function, opposite to (Ag)-10Al, and it has a final value of 729 MPa, the highest among the five metals, at the ending stage of uniform strain region.

Moreover, it is noticeable that the UTS values of all concentrated Ag solid solution alloys studied are similar to each other. Among them, (Ag)-10Ga has the largest value, namely, 246.1 MPa, which is 1.84 times of that of pure Ag. On the other hand, however, the values of true uniform strain are quite different from each other. (Ag)-10Al and (Ag)-8Sn have similar true uniform strain values, about 1.4 times of that of pure Ag. Impressively, (Ag)-10Ga has the largest value of true uniform strain among those concentrated Ag solid solution alloys with similar solute concentrations, which is 2.6 times of that of pure Ag. The true uniform strain value of (Ag)-10Ga surpasses the value of (Ag)-9.5In by 20%. It is safe to conclude that both ultimate mechanical strength and ductility of Ag can be increased significantly by alloying with the Ga solute element at relatively high concentration.

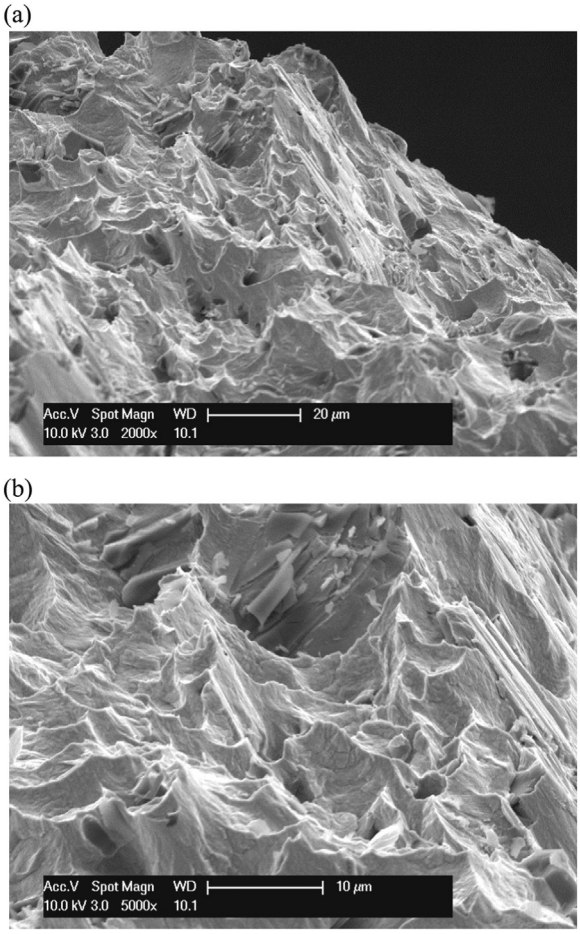

Fig. 6. Fractography of (Ag)-10Al representative tensile test sample, (a) SEM image at 2000 × magnification, (b) SEM image at 5000 × magnification.

3.4. Fractography

Topography of fracture surfaces of samples tested can provide some additional information and qualitatively described the deformation history of materials. The fractography of representative tensile test samples of (Ag)-10Al, (Ag)-10Ga and (Ag)-8Sn were examined under SEM at various fracture regions and different magnifications, in order to gain some insights of the deformation history from a microscopic point of view. As shown in Fig. 6, the morphology of fracture surface of (Ag)-10Al exhibits a feature called tear-ridges, which should be corresponding to quasi-cleavage fracture mode. Quasi-cleavage occurs where the crack initiates, and the fracture changes to intergranular as the crack grows. This type of fracture mode denotes that some but a limited amount of plastic deformation has occurred before failure, and it can be classified into the category of semi-ductile fracture morphology. The morphology of fracture surface of (Ag)-8Sn exhibits a smooth and fibrous-like feature in some regions, as shown in Fig. 7(a), or a shallow dimpled rupture feature in other regions, shown in Fig. 7(b). The morphology feature shown in Fig. 7(a) is not very typical, but it could be corresponding to transgranular fracture since it has a smooth looking and less sharp edges. Therefore, (Ag)-8Sn has a mixture fracture mode between brittle and ductile type in its nature. Although the elongations before the failure of (Ag)-10Al and (Ag)-8Sn tested samples are about the same, the opposite work hardening histories may explain the existing differences between their fractography. As shown in Fig. 8, the morphology of fracture surface of (Ag)-10Ga exhibits highly ductile character, since a large amount of necking, shown in Fig. 8(a), and many deep elliptical dimpled ruptures, shown in Fig. 8(b), have been observed. Microvoid formation and coalescence during the continued straining and plastic deformation are responsible for this dimpled rupture morphology [24], and shape of the dimples are depending on the local stress status during the tensile test. As seen in Fig. 3, the engineering strain of (Ag)-10Ga at fracture point is more than 80%, showing the truly remarkable elongation value. The topography of fracture surface of (Ag)-10Ga has testified that a large amount of plastic deformation has occurred before final failure, therefore, confirming that (Ag)-10Ga is indeed highly ductile in its nature.

3.5. Transmission electron microscopy results

In the literature, Ag-Al (7.5 at%) [25], Ag-In (11.5 at%) [26], and Ag-Sn (7.8 at%) [27], concentrated solid solution alloys with similar concentrations were studied under TEM in order to conduct the direct measurement for the stacking fault energy of those alloys from the observations of extended dislocations nodes in the micrographs. To the best knowledge of the authors, there is no direct TEM study reports on Ag-Ga solid solution alloy in the literature. As known from the tensile test and fractography results, (Ag)-10Ga has the highest ductility and highest ultimate strength, therefore, we decided focus our attention on Ag-Ga concentrated solid solution, using TEM direct observations, in order to investigate its microscopic structures and the underlying mechanism for the enhanced mechanical properties. The TEM sample was properly tilted and orientated with the guidance of FCC KiKuchi maps [28], in order to align up the [1 1 0] zone axis with the incident electron beam direction. As shown in Fig. 9(a), a representative global view of plastic deformed sample of (Ag)-10Ga was observed under TEM with relatively large area. A small aperture with the size of 500 nm in

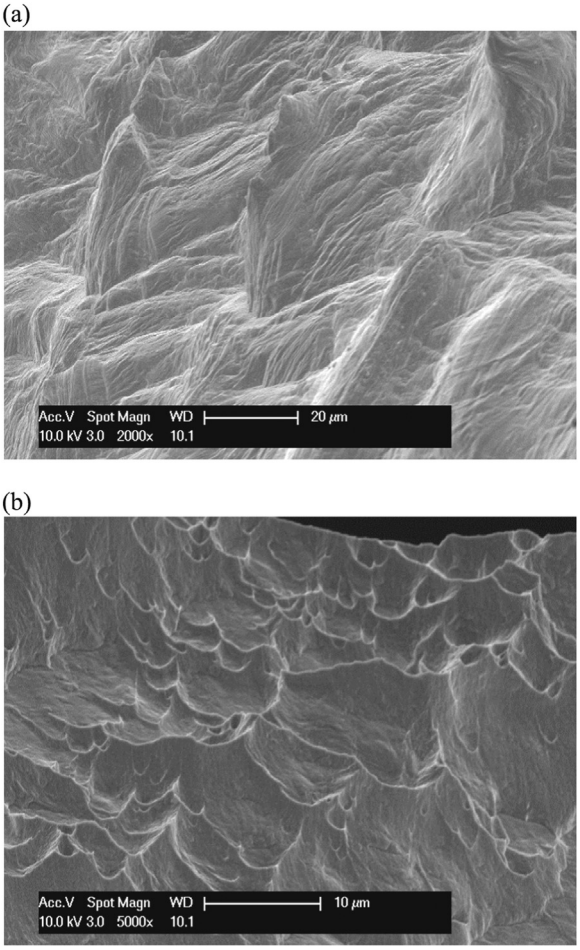

Fig. 7. Fractography of (Ag)-8Sn representative tensile test sample, (a) SEM image at **2000** × magnification, (b) SEM image at 5000 × magnification.

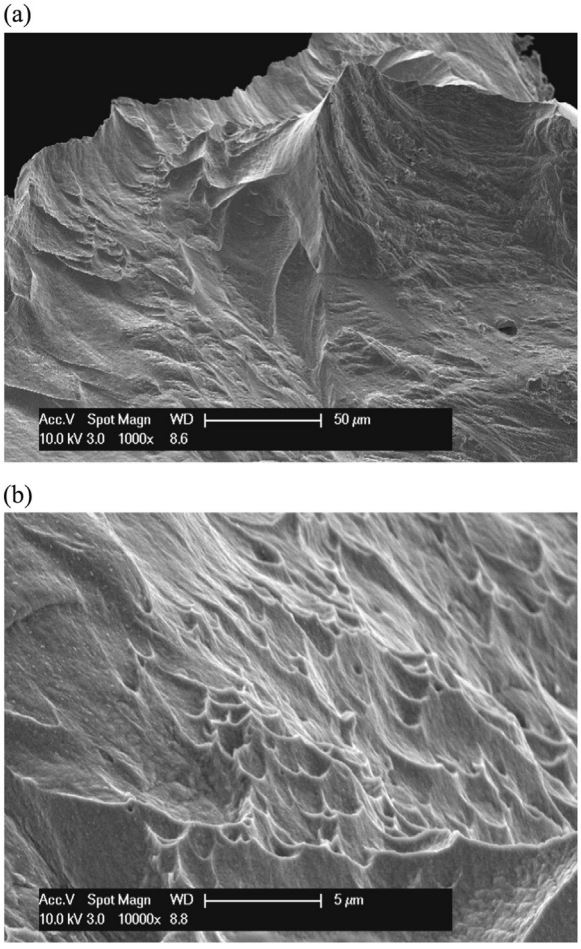

Fig. 8. Fractography of (Ag)-10Ga representative tensile test sample, (a) SEM image at 1000 × magnification, (b) SEM image at 10000 × magnification.

diameter was used to form selected area electron diffraction (SAED) pattern shown in the figure, thereby confirming the good align-up of the zone axis. Common TEM features in the deformed sample, as described in the literatures, can be seen in the micrograph, such as dislocation lines, grain boundaries, extended dislocations nodes, and stacking faults. Interestingly, a special feature in the micrograph has called our attentions. This feature is consisted of several sets of straight lines, crossing through the entire TEM micrograph from upper left region to bottom right region. A more localized view of this feature is shown in Fig. 9(b), as zoomed-in at the upper right corner of Fig. 9(a). By the visualization of SAED pattern for the whole area in Fig. 9(b), as shown in Fig. 9(c), we can safely interpret that this particular feature is corresponding to the twinning microstructures in the plastically deformed TEM sample. In the literature, the similar feature was also found in concentrated Ag-In (18.4 at%) solid solution alloy [29], and referred as the narrow twin lamellas. As shown in the schematics in Fig. 9(c), the twinning SAED patterns are formed by the superposition of individual SAED pattern of parent crystal and twinned crystal. Primarily, Fig. 9(c) is consisted of two sets of FCC [1 1 0] zone axis patterns (ZAPs), which are mirror-symmetrical with respect of the dotted yellow line. The dotted yellow line connects (-1 1 1) and (1-1-1) diffraction spots in Fig. 9(c), therefore aligning with the directions of (-1 1 1) or (1-1-1) plane normal vectors, i.e., g vectors in the reciprocal space. Therefore, the dotted yellow line is corresponding to the twinning plane in the SAED. As depicted in Fig. 9(c), we selected one pair of mirror-symmetrical spots in SAED, i.e., (0 0 2) and $(0\ 0\ 2)_T$, where subscript T stands for twinned, and drew line A and line B to connect them with the center transmitted electron spot. If we draw line C to connect (0 0 2) and $(0\ 0\ 2)_T$ spots, then line C should be perpendicular to the twinning plane. The angle φ forming by line A and line C is 35.5°, as measured in the SAED pattern, which is corresponding to the angle between (0 0 2) plane normal and the twinning direction. Therefore, the twinning direction is determined to be aligning along $< 1\ 1\ 2 >$ direction, so that it is safe to conclude that the deformation twinning is responsive to the formation of narrow twin lamellas in the TEM micrograph. As shown in Fig. 9(d), the classic twinning mechanism of FCC materials is clearly illustrated, in which deformation twins are created by stacking faults by three successive $1/6 < 1\ 1\ 2 >$ Shockley partial dislocations [30]. In the Fig. 9(d), the blue color stands for untwined zone, and red color stands twinned zone. In addition, one set of the twinning direction and the twining plane in real space are labelled in the schematic, corresponding to the reciprocal space twinning features of the SAED in Fig. 9(c).

As shown in Fig. 10(a), the high resolution TEM (HRTEM) micrograph of a single narrow twin lamella was taken at optimal Scherzer defocus condition, in which the bright spots correspond to phase contrast of individual atomic columns. The whole HRTEM image can be converted into a fast Fourier transformation (FFT) pattern, as shown in Fig. 10(b). It is clear that the FFT pattern resembles the twinning mirror symmetry nature in the SAED in Fig. 9(c). The width of a single narrow twin lamella is about 20 nm, and multiple twins are found within one single narrow twin lamella. The twin boundaries are parallel to one set of the {1 1 1} planes, and they are determined to be several atomic planes thick, caused by twinning partial dislocations that are tilted relatively to the electron beam, so that are not clearly imaged in the HRTEM micrograph. If we take a closer look at the red box labelled

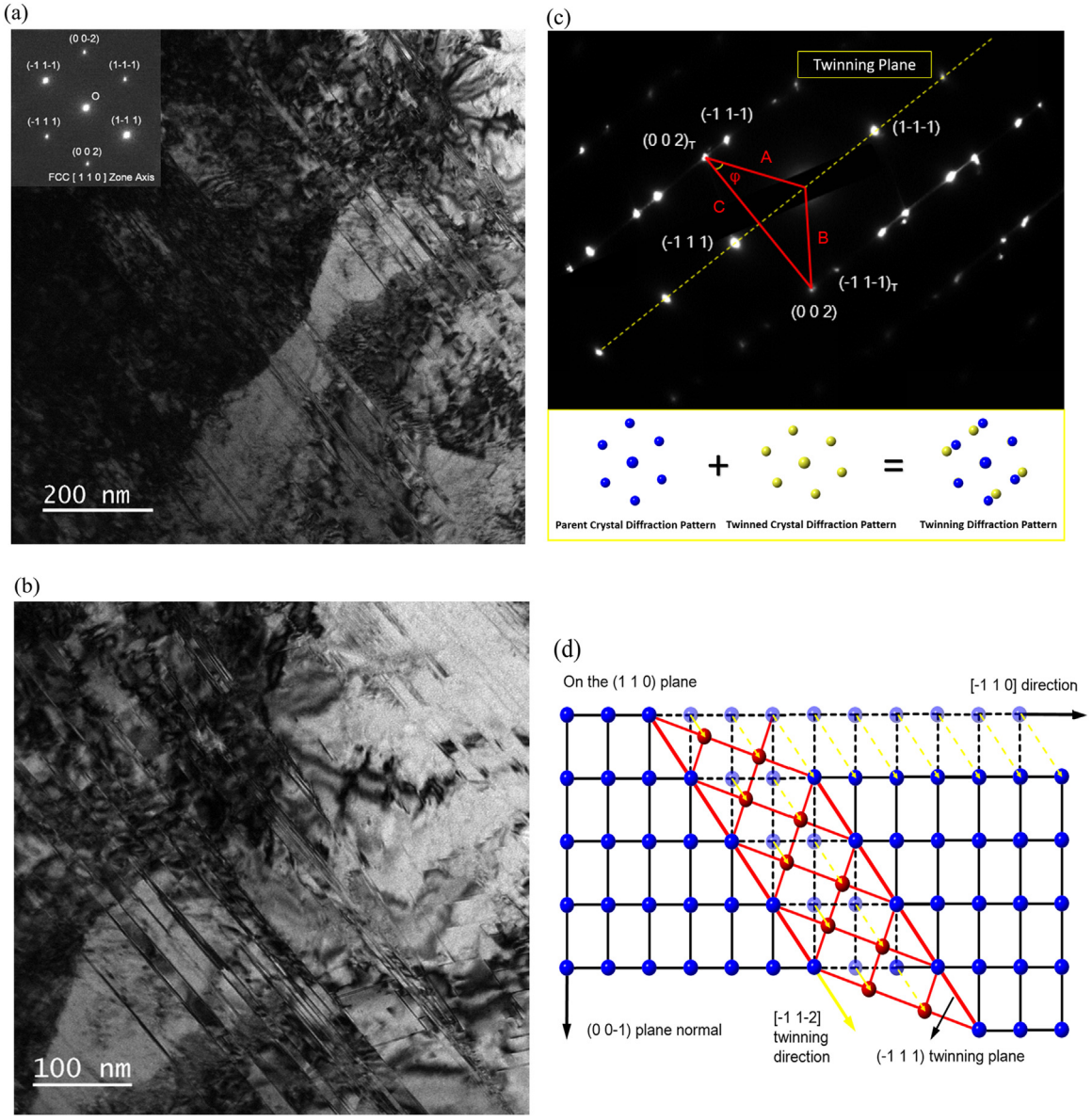

Fig. 9. (a) A representative global view of the TEM BF image for (Ag)-10Ga concentrated solid solution alloy, aligned-up with FCC [1 1 0] zone axis, (b) a more localized view of TEM BF image for the narrow twin lamellas structure in the (Ag)-10Ga concentrated solid solution alloy, (c) SAED pattern of the selected area in (b), showing the twinning diffraction pattern of the parent crystal and twinned crystal, as illustrated in the schematics, (d) a schematic diagram of the deformation twinning mechanism in FCC crystal lattice.

region of Fig. 10(a), an atomic resolution view can be seen at the boundary between parent crystal and twinned crystal region, as shown in Fig. 10(c). Dislocation cores can be directly observed at the boundary of narrow twin lamella, suggesting a direct interacting mechanism between dislocations and deformation twins might exist. The authors would like to conduct more discussions on the correlations between the macroscopic mechanical properties of concentrated Ag-based solid solution alloys and their corresponding microscopic mechanisms in the following session, regarding to the solid solution softening phenomenon and the enhanced ductility respectively.

4. Discussions

4.1. Solid solution softening

Generally, the phenomenon of solid solution softening may originate from intrinsic mechanism or extrinsic mechanism. In the latter one, the substitutional solute atoms have an indirect influence on the dislocation mobility due to the trapping of the interstitial impurities, often known as the scavenging effect, thereby suppressing the impurity segregation on the dislocations and grain boundaries [31]. However, the scavenging theory does not explain all of the experimental facts, where some solid solution softening phenomena show no strong sensitivity to the interstitial impurity level. Therefore, the intrinsic mechanism of solid solution softening was more popular and widely considered as the dominating factor in controlling the solid solution softening behaviors. The intrinsic mechanism of solid solution softening is essentially the direct interactions between substitutional solute atoms and the dislocations, resulting in the increase of dislocation mobility [12]. The physical models established in the early days described the effects of solute atoms on the movement of dislocations within a continuum elasticity theory, and consider the solute size misfit as a factor responsible for the solid solution softening. The difference of atomic radii or elastic moduli between solute and matrix atoms was referred as the solute size misfit factor, which might affect the distribution of Peierls potential [32]. In the current study, adding Al and Ga solute

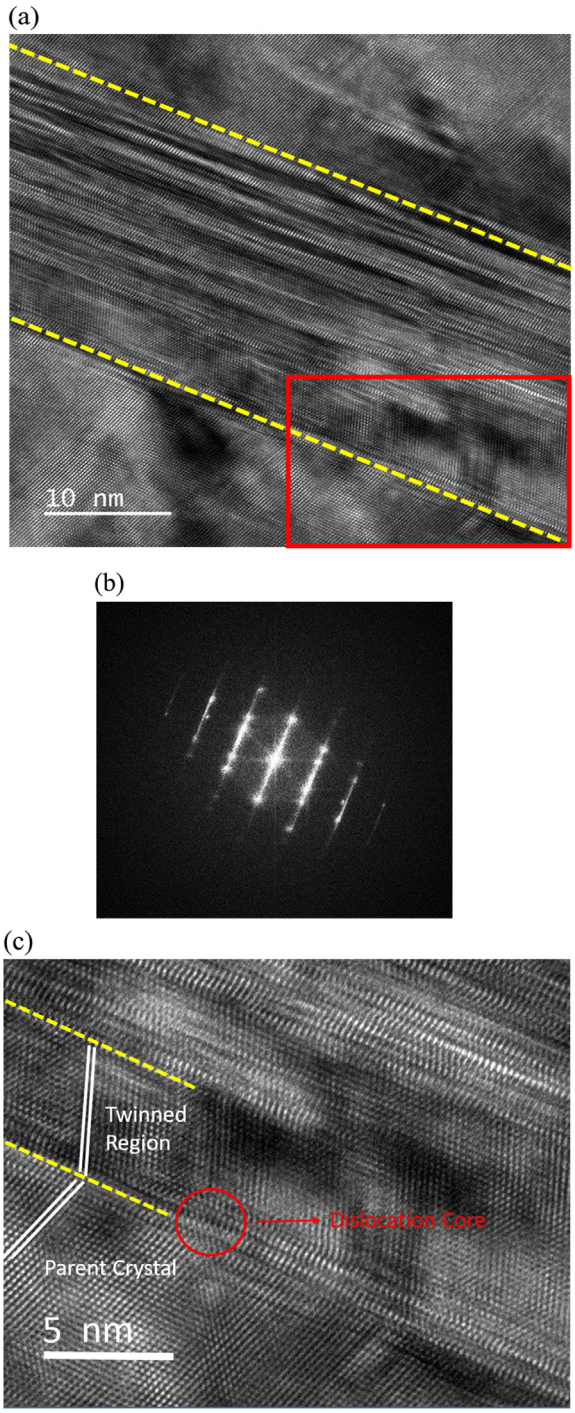

Fig. 10. (a) HRTEM image of a single twin lamella in the (Ag)-10Ga concentrated solid solution alloy, (b) the FFT pattern of a single twin lamella, (c) an atomic resolution view at the boundary between parent crystal and twinned crystal region.

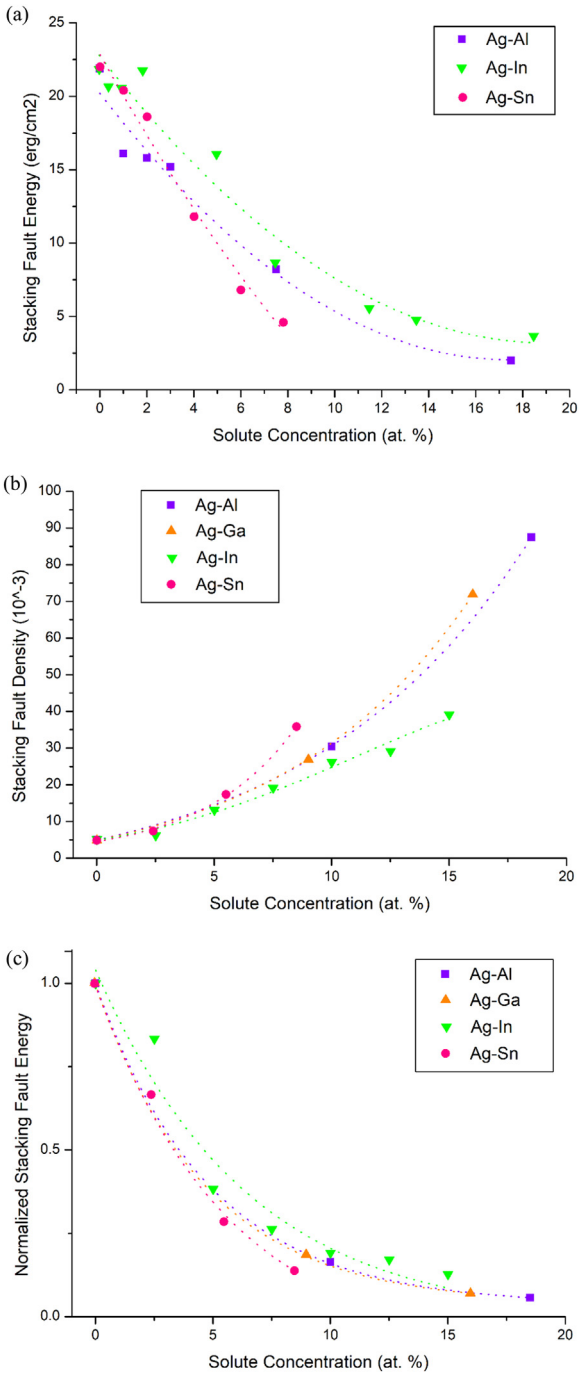

Fig. 11. (a) The variation of the intrinsic stacking fault energy with solute elements concentration in Ag-Al, Ag-In and Ag-Sn systems, using TEM extended nodes observation determined values [25–27], (b) the variation of the stacking fault density with solute elements concentration in Ag-Al, Ag-Ga, Ag-In and Ag-Sn systems, determined by XRD measurements [37], (c) the variation of the normalized intrinsic stacking fault energy with solute elements concentration in Ag-Al, Ag-Ga, Ag-In and Ag-Sn systems.

atoms resulted in compressive misfit strain centers in Ag crystal lattice, while adding In and Sn solute atoms resulted in dilating misfit strain centers, as indicated by the XRD experimental results. However, it is hard to find any correlations between the solute size misfit parameter and the mechanical behaviors of Ag-based FCC alloys. Since the strongest interaction between point defect and dislocation actually occurs inside the dislocation core, the continuum elasticity theorem, which was used by the previous physical model, is expected to be invalid. Experimentally, some previous results for BCC based alloys [33,34] indicated the same conclusion, i.e., size/modulus mismatches cannot solely explain the complex nature of solid solution softening behaviors.

Another perspective to interpret solid solution softening mechanism is inspired by one general trend based on the experimental facts that intrinsic stacking fault energy of solid solution alloy tends to decrease as the concentration of the solute element increases. This nature of solid solution alloys was well-recognized in many alloy systems, and systematically summarized by Gallagher in a review paper [35]. The

intrinsic stacking fault energy of pure Ag, γ_{Ag}, is 21.9 erg/cm^2, and the values of intrinsic stacking fault energy of solid solution alloys in Ag-Al [25], Ag-In [26] and Ag-Sn [27] systems were plotted as a function of solute concentration in Fig. 11 (a), using the values given in the literatures, as determined by the direct TEM measurements. Note that there is no record on the value of intrinsic stacking fault energy by the TEM measurement for the Ag-Ga system. Another parameter, called the stacking fault density, is the measure of the fraction of the whole surface of the close-packed planes occupied by the faults. It can be measured by X-ray diffraction methods [36], and is expected to be inversely proportional to the stacking fault energy. Therefore, the intrinsic stacking fault energy can be also calculated from the values of stacking fault density. The trends of stacking fault density vs. solute concentration in the Ag-Al, Ag-Ga, Ag-In and Ag-Sn systems [37] were depicted in Fig. 11 (b), and re-calculated values of stacking fault energy were further normalized with respect to the value of pure Ag, as plotted in Fig. 11(c). Clearly, the TEM direct measurement results are well-consistent with XRD indirect measurement results for the determination of intrinsic stacking fault energy in those Ag-based solid solution alloys. Both results indicate a strong dependence of intrinsic stacking fault energy on the solute concentration for all kinds of solute elements. The values of intrinsic stacking fault energy for (Ag)-10Al, (Ag)-9.5In, and (Ag)-8Sn can be obtained from the extrapolated (dotted) curves in Fig. 11(a), which are 5.2 erg/cm^2, 7.5 erg/cm^2, and 4.5 erg/cm^2, respectively. The normalized intrinsic stacking fault energy for (Ag)-10Al, (Ag)-10Ga, (Ag)-9.5In, and (Ag)-8Sn can be obtained from the extrapolated curves in Fig. 11(c), which are 0.164, 0.152, 0.221, and 0.139, respectively. Thus, value of the intrinsic stacking fault energy of (Ag)-10Ga can be roughly estimated, ranging from 4.5 erg/cm^2 to 5.2 erg/cm^2. Again, there is no direct causal correlation between the intrinsic stacking fault energies and the mechanical behaviors. However, an important insight can be gained, i.e., all of those concentrated Ag solid solution alloys have high probabilities to form intrinsic stacking fault, so that the full dislocations can be easily dissociated into Shockley partials with such low intrinsic stacking fault energies.

At a finite temperature, the dislocations will not move as straight line but rather by kink-pair formation. The existence of Bordoni peak [38] provides the evidence that kink-pair formation truly take place in FCC metals. Schoeck [39] has established a sophisticated physical model to analyze fractional kink-pair formation on dissociated dislocations for materials with low Peierls barrier, such as FCC metals, by using the generalized Peierls model [40]. Within the materials with low Peierls potential barrier, the dislocation can be moved by a successive formation of fractional kink-pairs with a much lower activation energy, compared with the one needed for the formation of the normal kink-pairs from full dislocations. The existence of fractional kink-pairs, running along < 1 1 2 > directions, could lead to a separate relaxation maximum at temperatures below the Bordoni peak, which has been observed in aluminum [41]. Mitchell [42] has proposed a physical model to examine the influences of stacking fault energy on nucleation and motion of fractional kink-pair on co-planar dissociated partial dislocations for the materials with high Peierls barrier, such as $MoSi_2$ intermetallics and $MgO\text{-}Al_2O_3$ ceramic spinel. The decrease in the localized value of the stacking fault energy near the solute atom was considered to have an influence on the dislocation core structure and to enhance the kink-pair nucleation. Even though this model is not directly applicable to low Peierls potential materials, the concepts of localized stacking fault energy variation due to the presence of the solute element and its influence on kink-pairs nucleation are inspiring. Medvedeva [43] has proposed the electronic origin of the intrinsic mechanism for the solid solution softening behaviors in BCC Mo-based alloys, based on the first-principle calculations. It has been shown that a strong correlation between the softening behaviors and the electronic valence band structures in binary Mo alloys exists [44]. The additions of solute elements can locally change the chemical bonding, reduce the energy barrier for double kinks nucleation, resulting in the enhancement the dislocation mobility. In the low Peierls potential FCC metals, the electronic origin may also play a dominant role in solid solution softening behaviors as well, but the fundamental mechanism could be different from the one in BCC metals. Although Al, Ga and In are elements all from IIIA column, their effective valence electron contributions to the mixing valence bands of solid solutions are considerably different from each other, in other words, not contributing all three outer shell electrons to the valence bands of the alloys.

Based on the arguments above, in here, a hypothesis is originally proposed in order to qualitatively explain the intrinsic solid solution softening mechanism for the low Peierls potential FCC materials, or in current case, for the concentrated Ag-based solid solution alloys. The melting temperatures (T_m) of solute elements of the current study are listed in a descending order as following: Al (933 K) > Sn (505 K) > In (430 K) > Ga (303 K). As shown in Fig. 4 and Table 2, the yield stress decreases as melting temperature of solute element decreases. At the room temperature (300 K), the homologous temperatures ($T_h = T/T_m$) of each solute element can be calculated and ordered as following: Al (0.32) < Sn (0.59) < In (0.70) < Ga (0.99). In the concentrated solid solution alloys, from statistical point of view, one would not expect to observe absolute random distribution of solute atoms in a substitutional solid solution with relatively high solute concentration. Rather, short range order (SRO) of arrangement of solute atoms would exist in the local area, even though the solid solution still is disordered in the long range. Therefore, the existence of SRO of solute atoms may affect the homologous temperature of some particular local area, resulting in the particular thermal-activated behaviors of materials. The homologous temperature of the specific local area is designated as localized homologous temperature (LHT). Since the formation process of double kink-pairs is commonly thermal-activated, the SRO local areas with higher localized homologous temperature can be easier sites for the fractional double kink-pairs nucleation. With the lower of the melting temperature of solute element, the localized homologous temperature is expected to be higher at the same ambient temperature, thereby facilitating the fractional double kink-pairs nucleation process. For the Ag-In and Ag-Ga concentrated solid solution, their LHT are expected to be significantly higher than pure Ag, and that could be one of the reasons why they demonstrated such prominent solid solution softening behaviors. On the other hand, Al solute element cannot significantly bring down the LHT. Therefore, SRO local areas, in this situation, would act as obstacle of dislocation gliding, same as what occurred in Ni-Cr concentrated FCC alloys [45], rather than the easier sites for the double kink-pairs nucleation. This resulted in solid solution hardening behaviors of the material. Since now SRO acted as an obstacle for dislocation gliding, once the leading dislocation had started to glide, the SRO would be destroyed and could not be restored, resulting in easier dislocation gliding in the crystal plane and relatively lower strain hardening rate. This explains the initial high stress hardening rate and later lowering stress hardening rate of (Ag)-10Al, as shown in Fig. 5. It is worthy noticing that the solid solution hardening mechanism for the concentrated solid solution is distinctly different from the traditional theory for dilute solid solution [3]. The mechanical behaviors of (Ag)-8Sn could be the mixture modes of those two competing mechanisms between the SRO areas and movement of dislocations mentioned above.

4.2. Enhanced ductility

As seen from the TEM results, it is evident that a large quantity of deformation twins have been formed in the concentrated Ag-In [29] and Ag-Ga solid solution alloys under a certain degree of plastic deformation. Therefore, the twinning-induced plasticity (TWIP) should be the corresponding mechanism for the enhanced ductility of Ag-In and Ag-Ga solid solution alloys. Twinning-induced plasticity is a well-known mechanism due to the competition between dislocation slip and deformation twinning [46], resulting in a combination of high strength

and excellent ductility. Typically, deformation twinning is commonly observed in hexagonal close-packed (HCP) crystal due to its inherent low number of active dislocation slip systems. TWIP is relatively rare for the FCC crystal structure materials, but it has been reported that deformation twinning can indeed occur in Ag-Au alloy at cryogenic temperature (77.3 K) [47] and in nano-crystalline Al [48] due to the suppression of the normal full dislocation gliding. If assuming the FCC deformation twins nucleate from perfect slip dislocations, an increase of the yield stress would be expected from a previous theoretical model [49], however, the current experimental facts have shown otherwise. Rather, it is expected that the formation of deformation twinning in Ag-In and Ag-Ga correlates with the Shockley partial dislocations and fractional kink-pair formation. As shown in Fig. 9(d), a successive formation of fractional kink-pairs on Shockley partial dislocations, running along the < 1 1 2 > directions, can be regarded as the embryo of deformation twins. The low intrinsic stacking fault energies of Ag-In and Ag-Ga can be attributed to the large deformation twinning formation tendency, but not exclusively. More quantitative approach to establish a rigorous theoretical interpretation must rely on atomistic simulation and the construction of generalized stacking fault energy surface (GSFE or γ surface) [39,40]. By the atomistic modelling, Li [50] has showed that four parameters can be derived from the construction of the γ surface, namely, intrinsic stacking fault energy (γ_{isf}), unstable stacking fault energy (γ_{usf}), unstable twin fault energy (γ_{utf}) and extrinsic stacking fault energy (γ_{esf}), and they are very useful in the understanding the nucleation mechanism of deformation twins in Cu-based alloys. Specialized in describing the randomness and chaotic nature of disordered solid solution within the density functional theory (DFT) regime, ab initio alloy theory formulated within the exact muffin-tin orbitals (EMTO) method [51] was used in that work. As shown in Eq. (6), a quantity to measure the twinnability, T, was proposed by Asaro [52] to interpret the competition between regular dislocation slip and deformation twinning. Based on this model, the deformation twinning is energetically favored over dislocation slip if T > 1, or vice versa.

$$T = \sqrt{(3\gamma_{usf} - 2\gamma_{isf})/\gamma_{utf}} \quad (6)$$

This quantum-mechanical methodology should be readily applicable to the concentrated Ag-based solid solution alloys as well. However, the atomistic modelling is beyond the scope of the current paper, so the authors would rather discuss more about the underlying mechanism quantitatively in twinning-induced plasticity in the future work.

5. Concluding remarks

In the semiconductor integration, packaging and manufacturing process, the relatively low hardness and yield strength are highly desirable material properties in the selection of interconnecting materials, because it induces less contact stress to the areas underneath bond pads on integrated circuit (IC) chips [53]. Lower yield strength can be beneficial to the rapid solid-state bonding process by allowing to achieve higher value of truly bonded fraction [54]. With lower yield strength and higher degree of ductility, the interconnecting material can also accommodate the CTE mismatch induced stress, which is very common and troublesome in the heterogeneous integration process, and release the thermal stress through the plastic deformation process.

In this paper, it has been discovered that (Ag)-10Ga possesses the material properties with most desirable combination for electronic device solid-state bonding applications, i.e., lowest yield strength, largest uniform strain (ductility) and highest UTS among those concentrated Ag solid solution alloys with similar solute concentrations. Furthermore, Ga has extremely low melting temperature, at 29.8 °C, and Ag-Ga eutectic temperature is even lower, at 25 °C. Therefore, it can be considered and to be explored as a new alternative method as transit liquid phase (TLP) bonding technique [55], using the Ag-Ga binary system. It could be a suitable candidate of low temperature (below 200 °C) or even room temperature bonding technique for advanced microelectronics, micro-electro-mechanical-systems (MEMS) and optoelectronic devices [56].

In summary, concentrated Ag-based solid solutions with Al, Ga, In and Sn solutes have been extensively investigated in terms of the phenomenological nature of their macroscopic mechanical behaviors and underlying microscopic mechanism. For the future research activity, it is suggested that ab initio calculation formulated within EMTO method can be applied to quantum-mechanically constructγsurface of the concentrated Ag-based solid solutions, thereby quantitatively modelling the formation of the deformation twinning. It is also suggested that the synchrotron XRD experimental study on the dislocation number density and in-situ TEM study on evolution of twin lamellas could be helpful to the further understanding of the solid solution softening behaviors and the enhanced ductility in FCC concentrated solid solution alloys.

Acknowledgement

The authors would like to acknowledge the XRD, SEM/EDX, and TEM works preformed in IMRI, using Rigaku SmartLab X-ray diffractometer, Philips XL-30 FEG SEM with EDS system and JEOL JEM-2100F TEM respectively. The authors would also like to express our gratitude towards the help from Prof. Farghalli Mohamed and Prof. Enrique Lavernia in facilitating the tensile test and TEM sample preparation, respectively, for our research activity.

References

[1] W. Hume-Rothery, G.F. Lewin, P.W. Reynolds, The lattice spacings of certain primary solid solutions in silver and copper, Proc. R. Soc. Lond. Ser. A Math. Phys. Sci. 157.890 (1936) 0167–0183.
[2] R. Bacon, C.S. Smith, Single crystal elastic constants of silver and silver alloys, Acta Metall. 4 (4) (1956) 337–341.
[3] R.L. Fleischer, Substitutional solution hardening, Acta Metall. 11 (3) (1963) 203–209.
[4] R.W.K. Honeycombe, The Plastic Deformation of Metals, First edition, Edward Arnold Ltd, Cambridge, 1968.
[5] P. Jax, P. Kratochvil, P. Haasen, Solid solution hardening of gold and other fcc single crystals, Acta Metall. 18 (2) (1970) 237–245.
[6] J.G. Bai, J. Yin, Z. Zhang, G.Q. Lu, J.D. van Wyk, High-temperature operation of SiC power devices by low-temperature sintered silver die-attachment, IEEE Trans. Adv. Packag. 30 (3) (2007) 506–510.
[7] Y.Y. Wu, C.C. Lee, The strength of high-temperature Ag–In joints produced between copper by fluxless low-temperature processes, J. Electron. Packag. 136 (1) (2014) 0110061–0110066.
[8] T.H. Chuang, C.H. Tsai, H.C. Wang, C.C. Chang, C.H. Chuang, J.D. Lee, H.H. Tsai, Effects of annealing twins on the grain growth and mechanical properties of Ag-8Au-3Pd bonding wires, J. Electron. Mater. 41 (11) (2012) 3215–3222.
[9] T.H. Chuang, H.C. Wang, C.H. Chuang, H.J. Lin, J.D. Lee, H.H. Tsai, Surface reconstruction of an annealing twinned Ag-8Au-3Pd alloy wire under current stressing, Metall. Mater. Trans. A 44 (11) (2013) 5106–5112.
[10] Y. Huo, C.C. Lee, The growth and stress vs. strain characterization of the silver solid solution phase with indium, J. Alloy. Compd. 661 (2016) 372–379.
[11] Y. Huo, J. Wu, C.C. Lee, Study of anti-tarnishing mechanism in Ag-In binary system by using semi-quantum-mechanical approach, J. Electrochem. Soc. 164 (7) (2017) C418–C427.
[12] A. Sato, M. Meshii, Solid solution softening and solid solution hardening, Acta Metall. 21.6 (1973) 753–768.
[13] A.A. Sharif, A. Misra, T.E. Mitchell, Deformation mechanisms of polycrystalline $MoSi_2$ alloyed with 1 at% Nb, Mater. Sci. Eng.: A 358 (1) (2003) 279–287.
[14] K. Maeda, S. Takeuchi, Enhancement of dislocation mobility in semiconducting crystals by electronic excitation, in: F.R.N. Nabarro (Ed.), Dislocations in Solids, 10 North-Holland, Amsterdam, 1996, pp. 443–504.
[15] T.E. Mitchell, Dislocations and mechanical properties of MgO-Al_2O_3 spinel single crystals, J. Am. Ceram. Soc. 82 (12) (1999) 3305–3316.
[16] J. Lau, Thermal Stress and Strain in Microelectronics Packaging, Springer Science & Business Media, 2012.
[17] A.R. Dhamdhere, A.P. Malshe, W.F. Schmidt, W.D. Brown, Investigation of reliability issues in high power laser diode bar packages, Microelectron. Reliab. 43 (2) (2003) 287–295.
[18] A.J. McAlister, The Ag-Al (silver-aluminum) system, Bull. Alloy Phase Diagr. 8 (6) (1987) 527–533.
[19] M.R. Baron, The Ag-Ga (silver-gallium) system, Bull. Alloy Phase Diagr. 11 (4) (1990) 334–339.
[20] I. Karakaya, W.T. Thompson, The Ag-Sn (silver-tin) system, Bull. Alloy Phase Diagr. 8 (4) (1987) 340–347.

[21] ASTM standard E8/ E8M- 08, Standard test methods for tension testing of metallic materials, ASTM International, West Conshohocken, PA, 2008⟨http://dx.doi.org/10.1520/E0008_E0008M-08⟩, ⟨www.astm.org⟩.
[22] G.E. Dieter, Mechanical Metallurgy, Third edition, Mc Graw Hill, NY, 1986.
[23] P. Dadras, S. Majlessi, Plastic bending of work hardening materials, J. Eng. Ind. (Trans. ASME) 104 (3) (1982) 224–230.
[24] R.H. Van Stone, T.B. Cox, J.R. Low Jr, J.A. Psioda, Microstructural aspects of fracture by dimpled rupture, Int. Met. Rev. 30.1 (1985) 157–179.
[25] A. Howie, P.R. Swann, Direct measurements of stacking-fault energies from observations of dislocation nodes, Philos. Mag. 6 (70) (1961) 1215–1226.
[26] P.C.J. Gallagher, J. Washburn, The stacking-fault energy in the Ag-In series, Philos. Mag. 14 (131) (1966) 971–978.
[27] A.W. Ruff, L.K. Ives, Dislocation node determinations of the stacking fault energy in silver-tin alloys, Acta Metall. 15 (2) (1967) 189–198.
[28] D.B. Williams, C.B. Carter, The Transmission Electron Microscope. Transmission Electron Microscopy, Springer, Boston, MA, 1996.
[29] V. Franetović, D. Kunstelj, A. Bonefačić, The investigation of metastable ζ-hcp phase in the Ag-rich fcc region of Ag-In alloys rapidly quenched from the melt, J. Mater. Sci. 17 (10) (1982) 2771–2780.
[30] J.B. Cohen, J. Weertman, A dislocation model for twinning in fcc metals, Acta Metall. 11 (8) (1963) 996–998.
[31] K.V. Ravi, R. Gibala, The strength of niobium-oxygen solid solutions, Acta Metall. 18 (6) (1970) 623–634.
[32] R. Peierls, The size of a dislocation, Proc. Phys. Soc. 52 (1) (1940) 34–37.
[33] E. Pink, R.J. Arsenault, Low-temperature softening in body-centered cubic alloys, Prog. Mater. Sci. 24 (1980) 1–50.
[34] K. Okazaki, Solid-solution hardening and softening in binary iron alloys, J. Mater. Sci. 31 (4) (1996) 1087–1099.
[35] P.C.J. Gallagher, The influence of alloying, temperature, and related effects on the stacking fault energy, Metall. Trans. 1 (9) (1970) 2429–2461.
[36] R.G. Davies, R.W. Cahn, Stacking fault densities in filings of some copper-and silver-base solid solutions, Acta Metall. 10 (6) (1962) 621–624.
[37] L. Delehouzee, A. Deruyttere, The stacking fault density in solid solutions based on copper, silver, nickel, aluminium and lead, Acta Metall. 15 (5) (1967) 727–734.
[38] G. Fantozzi, C. Esnouf, W. Benoit, I.G. Ritchie, Internal friction and micro-deformation due to the intrinsic properties of dislocations: the Bordoni relaxation, Prog. Mater. Sci. 27 (3–4) (1982) 311–451.
[39] G. Schoeck, Normal and fractional kink pairs in dissociated dislocations, Philos. Mag. A 82 (5) (2002) 1033–1048.
[40] V. Vitek, Intrinsic stacking faults in body-centred cubic crystals, Philos. Mag. 18 (154) (1968) 773–786.
[41] T. Kosugi, T. Kino, A new low-temperature dislocation-relaxation peak in aluminum, J. Phys. Soc. Jpn. 58 (12) (1989) 4269–4272.
[42] T.E. Mitchell, P.M. Anderson, M.I. Baskes, S.P. Chen, R.G. Hoagland, A. Misra, Nucleation of kink pairs on partial dislocations: a new model for solution hardening and softening, Philos. Mag. 83 (11) (2003) 1329–1346.
[43] N.I. Medvedeva, Y.N. Gornostyrev, A.J. Freeman, Electronic origin of solid solution softening in bcc molybdenum alloys, Phys. Rev. Lett. 94 (13) (2005) 136402.
[44] N.I. Medvedeva, Y.N. Gornostyrev, A.J. Freeman, Solid solution softening in bcc Mo alloys: effect of transition-metal additions on dislocation structure and mobility, Phys. Rev. B 72 (13) (2005) (pp. 134107-1-9).
[45] N. Clement, D. Caillard, J.L. Martin, Heterogeneous deformation of concentrated Ni-Cr FCC alloys: macroscopic and microscopic behavior, Acta Metall. 32 (6) (1984) 961–975.
[46] Y.Y. Wang, X. Sun, Y.D. Wang, X.H. Hu, H.M. Zbib, A mechanism-based model for deformation twinning in polycrystalline FCC steel, Mater. Sci. Eng.: A 607 (2014) 206–218.
[47] H. Suzuki, C.S. Barrett, Deformation twinning in silver-gold alloys, Acta Metall. 6 (3) (1958) 156–165.
[48] M. Chen, E. Ma, K.J. Hemker, H. Sheng, Y. Wang, X. Cheng, Deformation twinning in nanocrystalline aluminum, Science 300 (5623) (2003) 1275–1277.
[49] L. Remy, Kinetics of FCC deformation twinning and its relationship to stress-strain behaviour, Acta Metall. 26 (3) (1978) 443–451.
[50] W. Li, S. Lu, Q.M. Hu, S.K. Kwon, B. Johansson, L. Vitos, Generalized stacking fault energies of alloys, J. Phys.: Condens. Matter 26 (26) (2014) (pp. 265005-1-12).
[51] L. Vitos, Computational Quantum Mechanics for Materials Engineers: The EMTO Method and Applications, Springer Science & Business Media, 2007.
[52] R.J. Asaro, S. Suresh, Mechanistic models for the activation volume and rate sensitivity in metals with nanocrystalline grains and nano-scale twins, Acta Mater. 53 (12) (2005) 3369–3382.
[53] Z.W. Zhong, H.M. Ho, Y.C. Tan, W.C. Tan, H.M. Goh, B.H. Toh, J. Tan, Study of factors affecting the hardness of ball bonds in copper wire bonding, Microelectron. Eng. 84 (2) (2007) 368–374.
[54] G. Chen, Z. Feng, J. Chen, L. Liu, H. Li, Q. Liu, S. Zhang, X. Cao, G. Zhang, Q. Shi, Analytical approach for describing the collapse of surface asperities under compressive stress during rapid solid state bonding, Scr. Mater. 128 (2017) 41–44.
[55] R.W. Chuang, C.C. Lee, Silver-indium joints produced at low temperature for high temperature devices, IEEE Trans. Compon. Packag. Technol. 25 (3) (2002) 453–458.
[56] E. Higurashi, T. Suga, Review of low-temperature bonding technologies and their application in optoelectronic devices, Electron. Commun. Jpn. 99 (3) (2016) 63–71.